SANDIA REPORT

SAND2006-4313
Unlimited Release
Printed September 2006

Mixing in Polymeric Microfluidic Devices

Christopher M. Brotherton, Robert H. Davis, Amy C. Sun, and P. Randall Schunk

Prepared by
Sandia National Laboratories
Albuquerque, New Mexico 87185 and Livermore, California 94550

Sandia is a multiprogram laboratory operated by Sandia Corporation,
a Lockheed Martin Company, for the United States Department of Energy's
National Nuclear Security Administration under Contract DE-AC04-94-AL85000.

Approved for public release; further dissemination unlimited.

Sandia National Laboratories

Issued by Sandia National Laboratories, operated for the United States Department of Energy by Sandia Corporation.

NOTICE: This report was prepared as an account of work sponsored by an agency of the United States Government. Neither the United States Government, nor any agency thereof, nor any of their employees, nor any of their contractors, subcontractors, or their employees, make any warranty, express or implied, or assume any legal liability or responsibility for the accuracy, completeness, or usefulness of any information, apparatus, product, or process disclosed, or represent that its use would not infringe privately owned rights. Reference herein to any specific commercial product, process, or service by trade name, trademark, manufacturer, or otherwise, does not necessarily constitute or imply its endorsement, recommendation, or favoring by the United States Government, any agency thereof, or any of their contractors or subcontractors. The views and opinions expressed herein do not necessarily state or reflect those of the United States Government, any agency thereof, or any of their contractors.

Printed in the United States of America. This report has been reproduced directly from the best available copy.

Available to DOE and DOE contractors from
U.S. Department of Energy
Office of Scientific and Technical Information
P.O. Box 62
Oak Ridge, TN 37831

Telephone: (865) 576-8401
Facsimile: (865) 576-5728
E-Mail: reports@adonis.osti.gov
Online ordering: http://www.osti.gov/bridge

Available to the public from
U.S. Department of Commerce
National Technical Information Service
5285 Port Royal Rd.
Springfield, VA 22161

Telephone: (800) 553-6847
Facsimile: (703) 605-6900
E-Mail: orders@ntis.fedworld.gov
Online order: http://www.ntis.gov/help/ordermethods.asp?loc=7-4-0#online

SAND2006-4313
Unlimited Release
Printed September 2006

Mixing in Polymeric Microfluidic Devices

Christopher M. Brotherton
University of Colorado at Boulder
Boulder, CO 80309
christopher.brotherton@colorado.edu

Robert H. Davis
University of Colorado at Boulder
Boulder, CO 80309
robert.davis@Colorado.EDU

Amy C. Sun
Multiphase Transport Processes
Sandia National Laboratories
P.O. Box 5800
Albuquerque, NM 87185-0835
acsun@sandia.gov

P. Randall Schunk
Multiphase Transport Processes
Sandia National Laboratories
P.O. Box 5800
Albuquerque, NM 87185-0835
prschun@sandia.gov

Abstract

This SAND report describes progress made during a Sandia National Laboratories sponsored graduate fellowship. The fellowship was funded through an LDRD proposal. The goal of this project is development and characterization of mixing strategies for polymeric microfluidic devices. The mixing strategies under investigation include electroosmotic flow focusing, hydrodynamic focusing, physical constrictions and porous polymer monoliths. For electroosmotic flow focusing, simulations were performed to determine the effect of electroosmotic flow in a microchannel with heterogeneous surface potential. The heterogeneous surface potential caused recirculations to form within the microchannel. These recirculations could then be used to restrict two mixing streams and reduce the characteristic diffusion length. Maximum mixing occurred when the ratio of the mixing region surface potential to the average channel surface potential was made large in magnitude and negative in sign, and when the ratio of the characteristic convection time to the characteristic diffusion time was minimized. Based on these results, experiments were performed to evaluate the manipulation of surface potential using living-radical photopolymerization. The material chosen to manipulate typically exhibits a negative surface potential. Using living-radical surface grafting, a positive surface potential was produced using 2-(Dimethylamino)ethyl methacrylate and a neutral surface was

produced using a poly(ethylene glycol) surface graft. Simulations investigating hydrodynamic focusing were also performed. For this technique, mixing is enhanced by using a tertiary fluid stream to constrict the two mixing streams and reduce the characteristic diffusion length. Maximum mixing occurred when the ratio of the tertiary flow stream flow-rate to the mixing streams flow-rate was maximized. Also, like the electroosmotic focusing mixer, mixing was also maximized when the ratio of the characteristic convection time to the characteristic diffusion time was minimized. Physical constrictions were investigated through simulations. The results show that the maximum mixing occurs when the height of the mixing region is minimized. Finally, experiments were performed to determine the effectiveness of using porous polymer monoliths to enhance mixing. The porous polymer monoliths were constructed using a monomer/salt paste. Two salt crystal size ranges were used; 75 to 106 microns and 53 to 180 microns. Mixing in the porous polymer monoliths fabricated with the 75 to 106 micron salt crystal size range was six times higher than a channel without a monolith. Mixing in the monolith fabricated with the 53 to 180 micron salt crystal size range was nine times higher.

Acknowledgments

The authors would like to acknowledge fellowships from Sandia National Laboratories and the U.S. Department of Education's Graduate Assistantships in Areas of National Need (GAANN) program.

The authors would also like to acknowledge Harry Rowland for his assistance with simulations; Brian Good and Tommy Haraldsson for their assistance with the CLiPP process and guidance; Robert Sebra for his help with living-radical photopolymerization surface grafting; Helen Simms for her assistance with porous polymer monoliths; Noeon Park and Jaeweon Cho for measuring zeta potentials; and members of the Robert H. Davis research group and the Multiphase Transport Processes Department for their help with simulations as well as experiments.

Contents

1 Overview 11
2 Background 13
2.1 Mixing using electroosmosis 13
2.2 Mixing using hydrodynamic focusing 14
2.3 Mixing using physical constrictions 15
2.4 Mixing using porous polymer monoliths 15
3 Analysis 17
3.1 Mixing using electroosmosis 17
3.2 Mixing using hydrodynamic focusing 22
3.3 Mixing using physical constrictions 24
3.4 Mixing using porous polymer monoliths 26
4 Recommendations 29
4.1 Porous polymer monoliths 29
4.2 Hydrodynamic focusing mixer 29
4.3 Microfluidic mixer comparison 29
References 33

Figures

1 This figure illustrates the two-dimensional electroosmotic flow mixer. The channel geometry has three inlets/outlets. Inlet A is a stream without solute. Inlet B is a stream with solute. C is the outlet. The channel is made up of four separate regions. Each region is labeled along with the zeta potential for each region. Region 3 is the mixing region. The analysis points are illustrated on figure with two solid black lines. The lines are located one channel height before the mixing region and one channel height after the mixing region. Each line represents multiple nodes. Each node has a result for pressure, velocity, and concentration. The EOM is calculated using the concentration data from the nodes. This figure is not to scale. 19

2 Extent of mixing (EOM) versus zeta potential ratio for a electroosmotic flow mixer. The length of the inlet stream (region 2) is ten times the height of the channel. The mixing region (region 3) has a length that is ten times the height of the channel. Each line represents a different modified Peclet number, Pe_m. In this figure, the modified Peclet number has values of 10, 33, 50, 66, 100, 150 and 200 (top to bottom). EOM increases with decreasing modified Peclet number and decreasing zeta potential ratio. 20

3 Zeta potential versus pH for the substrate (control), the substrate with a DMAEMA surface graft and the substrate with a PEG375 acrylate surface graft. The error bars represent the 90% confidence limits. The substrate was polymerized at 45 mW/cm^2 for 500 seconds. The surface grafts were polymerized at 45 mW/cm^2 for 900 seconds. The zeta potential measurements were conducted in a 10 mM KCl solution. 21

4 Zeta potential versus pH for substrate surface grafted with DMAEMA for various exposure times. The error bars represent the 90% confidence limits. The substrate was polymerized at 45 mW/cm^2 for 500 seconds. The surface grafts were polymerized at 45 mW/cm^2 for 0 (Control), 50, 100, 200, 450 and 900 seconds. The zeta potential measurements were conducted in a 10 mM KCl solution. 22

5 This figure illustrates the two-dimensional hydrodynamic focusing mixer. The channel geometry has five inlets/outlets. Inlet A is stream without solute. Inlet B is a stream with solute. Inlet C is an inlet. D and E are outlets. The channel has five labeled regions. Region 5 is the loop side channel and is not shown. The analysis points are illustrated on figure with two solid black lines. The analysis lines are located one channel height before the mixing region and one height after the mixing region. Each line represents multiple nodes. Each node has a result for pressure, velocity, and concentration. The concentration of the side channel outlet is averaged and then used as the side channel inlet boundary condition for the next iterations. The iterations continue until the difference in the average side channel outlet concentration for subsequent iterations is less than 0.01%. This figure is not to scale. 23

6 Extent of mixing (EOM) versus flow-rate ratio for a hydrodynamic focusing mixer with a loop side channel. The length of the inlet stream (region 2) is ten times the height of the channel. The mixing region (region 3) has a length that is ten times the height of the channel. Each line represents a different modified Peclet number, Pe_m. In this figure, the modified Peclet number has values of 10, 33, 50, 66, 100, 150 and 200 (top to bottom). EOM increases with decreasing modified Peclet number and increasing flow-rate ratio. 24

7 This figure illustrates the physical constriction mixer. The channel geometry has three inlets/outlets. Inlet A is stream without solute. Inlet B is a stream with solute. C is the outlet. The channel is made up of four regions. Region 3 is the mixing region. The height of the channel and the height of the constriction are labeled. The analysis points are illustrated on figure with two solid black lines. The analysis lines are located one unconstricted channel height before the mixing region and one unconstricted channel height after the mixing region. Each line represents multiple nodes. Each node has a result for pressure, velocity, and concentration. The EOM is calculated using the concentration data from the nodes. This figure is not to scale. 25

8 Extent of mixing (EOM) versus height ratio for a physical constriction mixer. The length of the inlet stream (region 2) is ten times the height of the channel. The mixing region (region 3) has a length that is ten times the height of the channel. Each line represents a different modified Peclet number, Pe_m. In this figure, the modified Peclet number has values of 10, 33, 50, 66, 100, 150 and 200 (top to bottom). EOM increases with decreasing modified Peclet number and decreasing height ratio. 25

9 Extent of mixing versus flow-rate for porous polymer monolith mixers. The control data set is for a straight channel without a polymer monolith. Two different monolith data sets are provided, each with a different pore size distribution. For the conditions investigated, the extent of mixing increases with increasing monolith heterogeneity, but is independent of the flow-rate. 27

1 Overview

Microfluidics is the study of fluid transport where the characteristic channel cross-sectional dimensions are on the order of tens to hundreds of microns. Microfluidics has broad applicability and is used in fields such as chemical and biological analysis, environmental monitoring and biotechnology. The advantages of using microfluidics stem from increased surface area to volume ratio, decreased reagent consumption, increased sensitivity, rapid results and portability [1–3]. Microfluidic research can be divided in to three areas: device fabrication methods [1, 3–7], fundamental investigation of fluid and particle transport [8] and systems of integrated unit operations [9]. A major goal for microfluidics is to combine the three main areas and fabricate self-contained "labs-on-a-chip". To accomplish this goal, several obstacles must be overcome. One such obstacle is mixing. On the microfluidic size scale, the flow is laminar and diffusion must be relied upon for mixing. Typically, diffusion is slow and effective ways to mix in the microfluidic environment must be identified.

The goal of this project is development and characterization of mixing strategies for polymeric microfluidic devices. This project identifies mixer designs that can be fabricated using the contact liquid photopolymerization process and investigates these designs with both numerical simulations and experimentation. The main objectives of this research are:

1. To determine the feasibility of using electroosmotic flow with surface-grafted channels as a microfluidic mixer,
2. To investigate the use of hydrodynamic focusing as a mixing technique,
3. To investigate the use of physical constrictions to enhance mixing, and
4. To investigate the use of porous polymer monoliths as microfluidic mixers.

2 Background

The first microfluidic devices were researched in the 1980s and are referred to as micro-electro-mechanical systems (MEMS). MEMS are typically made from glass or silicon and use mechanical devices such as actuators and pumps. MEMS eventually spawned miniaturized total analytical systems, which are tiny laboratories used for reactions and analysis. These analytical devices are commonly referred to as ”labs-on-a-chip” and have wide-ranging applications. One of the most interesting application is the use of labs-on-a-chip to help diagnose disease and detect chemical/biological contamination [10, 11].

One particularly challenging aspect of microfluidics is mixing. Since microfluidic flow is typically laminar in nature, diffusion must be relied upon for mixing [12]. Two recent review articles by Nguyen et. al. [13] and Hessel et. al. [14] discuss the current state of microfluidic mixers. In microfluidics, mixing techniques can be separated into two separate categories; passive and active. A passive mixer is defined as a mixer that does not require any external power. The only energy necessary to operate the mixer is the energy associated with producing the required pressure drop. An active mixer utilizes an external power source. Each category can then be broken down into separate subcategories. For passive mixers, the subcategories are lamination, injection, chaotic advection and droplet. For active mixers, the subcategories are electrohydrodynamic, dielectrophoretic, electrokinetic, magneto hydrodynamic, acoustic, thermal and pressure disturbances. In all cases, the goal of micromixers is to increase the concentration gradient or the contact area between the two mixing liquids.

The work presented here has focused on investigating both active and passive mixers that can be incorporated into the microfluidic platform developed at the University of Colorado in Boulder. The microfluidic fabrication platform uses the contact liquid photopolymerization (CLiPP) process. The CLiPP process uses living radical photopolymerization (LRP) and allows for complex geometries and surface modification in microfluidic devices. Mixing techniques were selected that use the fabrication capabilities of the CLiPP process [4, 15]. The mixing techniques selected are mixing in channels with step changes in zeta potential driven by electroosmotic flow, mixing in channels constricted by hydrodynamic focusing, mixing in channels with physical constrictions and mixing with porous polymer monoliths.

2.1 Mixing using electroosmosis

An electroosmotic flow mixer was selected for investigation since LRP can be used to modify the surface chemistry of microfluidic channels. Electroosmosis describes flow of an electrolyte, due to an applied voltage or electric field, through a channel with charged surfaces. The problem is simplified for typical situations where the Debye layer of counter ions adjacent to the charged walls is thin compared with the channel width and height. In this case, electroosmosis provides a slip velocity parallel to the channel walls [16]:

$$v = -\frac{\varepsilon \zeta E_t}{\mu} , \tag{1}$$

where ε is the dielectric constant of the fluid, ζ is the zeta potential of the surface, E_t is the tangential component of the electric field (voltage per unit length) at the channel walls, and μ is the fluid viscosity. This velocity occurs at the edge of the Debye layer, but it can be effectively applied as a boundary condition at the channel wall when the Debye layer is sufficiently thin.

For a uniform electric field, fixed zeta potential, and constant channel cross section, the fluid moves through the channel with a plug-flow profile, with the velocity given by Eq. (1). However, if the electric field, channel cross section, or zeta potential are not constant then complex flow profiles can be expected. Oddy et. al. [17] investigated using periodic electric potentials oriented perpendicular to the flow. The potentials lead to electrokinetic instabilities that disrupted the laminar nature of the flow and increased mixing. One popular method for manipulating electroosmotic flow is to modify the surfaces of the microfluidic channels [18–27]. Since electroosmotic flow is proportional to the zeta potential of a surface, modifying the zeta potential on that surface can be an effective way to manipulate electroosmotic velocity. One interesting example is to modify the channel surface only within a certain region of the channel, so that the zeta potential in that region is opposite the zeta potential of the rest of the channel. The slip velocity within the modified region is in the opposite direction of the overall flow, causing recirculations. These recirculations will constrict two mixing streams, which decreases the characteristic diffusion length and increases mixing.

Previous research used coatings within silicon channels to cause recirculations. The coatings were effective, but difficult to use [28]. Research has also been performed to investigate the effect of zeta potential patterns on mixing in an electroosmotic pump. The highest mixing occurred when the surface-grafted channel walls were opposite each other and were used to constrict the mixing fluids [29]. Chang et. al. [30] expanded on this research and included blocks within the channel. The block caused further constriction of the mixing streams and led to even higher mixing. Wu et. al. [31] combined the idea of heterogeneous zeta potential with embedded electrodes of novel configurations that produced a mixing efficiency near 90%. Patterned zeta potentials also have a disadvantage. The overall flow-rate is proportional to the average zeta potential. Utilizing patterned zeta potentials may increase mixing, but requires a higher electric potential for a constant flow-rate [32]. The research presented here has focused on both understanding the mixing that occurs in electroosmotic pumps with patterned zeta potential and performing proof-of-concept experiments to investigate how LRP can be used to manipulate the zeta potentials in a controlled fashion.

2.2 Mixing using hydrodynamic focusing

Hydrodynamic focusing is the process where a liquid stream is constricted by an adjacent liquid stream. Work by Jenson [33, 34] revealed that fast mixing can be achieved by constricting mixing streams using hydrodynamic focusing. Results showed that constricting the mixing streams down to 50 nm resulted in a 10 microsecond mixing time. These results are particularly significant because the fast mixing times make investigation into chemical reactions with quick reaction times possible. Research presented here investigates hydrodynamic focusing mixing on a larger size scale. Instead of constricting the mixing streams down to nanometer size scales, the results presented here illustrate constrictions on the order of microns. The mixing times will therefore be

longer, but the required pressure drop will be less.

2.3 Mixing using physical constrictions

Instead of relying on a step change in zeta potential or a secondary liquid stream, decreasing the characteristic diffusion length can also be established by using a constriction in the cross section of the microfluidic channel. The disadvantage of using physical constrictions is that the constriction height must always be larger than the average diameter of any particles or cells that are in the fluid. The other two mixers (electroosmosis and hydrodynamic focusing) do not have this restriction. Veenstra et. al. [35] demonstrated that mixing can be increased by imposing a physical constriction within the channel. Results were presented for the characteristic diffusion time versus channel width and the pressure drop versus channel width for a given channel length. The characteristic diffusion time decreased with decreasing channel width and the pressure drop increased with decreasing width. The authors did not consider varying the length of the constriction. By increasing the length of the constriction, the amount of time the mixing liquids are constricted increases, leading to increased mixing. The work present here expands on this study and investigates the effect of channel height, channel length, solute diffusivity and volumetric flow-rate on mixing.

2.4 Mixing using porous polymer monoliths

Porous polymer monoliths are used to disrupt the laminar nature of microfluidic flows. Porous mixers are considered passive mixers and are often compared with packed bed mixers or with mixers that use structures within the microchannels. Common fabrication techniques for porous monoliths uses phase separation photopolymerization [36–40]. These studies have focused on controlling the pore properties within the monoliths. The pores sizes fabricated ranged from on the order of nanometers to on the order of microns. In each case, the monomer composition and material selection was varied to control the final mean pore size. Rohr et. al. [36] studied the effectiveness of porous monoliths on mixing in microfluidic devices. They found that the best mixing occurred in monoliths with large irregular pores. Work presented here focuses on porous polymer monoliths fabricated using a salt crystal/monomer mixture described in Simms et. al. [41]. By using salt, the pore size distribution can be more easily tailored and fabrication is simpler.

3 Analysis

3.1 Mixing using electroosmosis

The projects in this section describe research on electroosmotic flow as a mixing technique. Results presented here illustrate designing electroosmotic mixers and proof-of-concept experiments that investigate the effectiveness of LRP surface grafting to manipulate the zeta potential of the fabrication substrate material.

3.1.1 Mixing utilizing electroosmosis in channels with step changes in zeta potential

Previous work investigating electroosmosis with step changes in zeta potential and cross section revealed that the velocity profiles within the different regions can be manipulated [27]. This study investigates step changes in zeta potential that cause recirculating flow profiles. The recirculating flow profiles can be used to constrict fluids and increase mixing.

GOMA, a piece of finite element computational software written at Sandia National Laboratories, was used for the simulations. GOMA is a finite element program capable of coupled transport (momentum, heat and mass) problems in two- and three-dimensions. Additionally, GOMA is capable of solving problems that include free or moving boundaries between different materials or phases. This problem was solved using the two-dimensional equations for continuity, Navier-Stokes, mass transfer and voltage. At the channel walls the solute flux is zero, the normal component of velocity is zero and the tangential component of velocity is equal to the electroosmotic velocity. The electroosmotic slip velocity boundary condition is valid in channels with sufficiently small Debye layers. The inlet and outlet of the channel are assigned voltages to determine the voltage drop within the channel.

To evaluate electroosmosis for mixing, a quantitative measure of the extent of mixing (EOM) must be defined. The EOM is calculated by comparing the concentration profile of the solute before and after the mixer. The concentration versus channel position profiles are split into two regions. The first region represents the top half of the channel and the second region represents the bottom half of the channel. The concentration in each region is integrated over the channel half-width. The integral of the top region is subtracted from the integral of the bottom region. Mathematically, the difference is

$$\Delta = \int_0^{\frac{H}{2}} C dy - \int_{\frac{H}{2}}^{H} C dy \,, \tag{2}$$

where H is the height of the channel. The above equation is evaluated for both the concentration profiles before and after the mixer. The final extent of mixing (EOM) is calculated using

$$\text{EOM} = 1 - \frac{\Delta O}{\Delta I} \,, \tag{3}$$

where ΔO is determined using the concentration profile after the mixing region and ΔI is determined using the concentration profile before the mixing region. An EOM of 1 represents perfect mixing and a value of 0 represents no mixing.

To investigate electroosmosis for mixing, a dimensional analysis was performed to determine the important dimensionless groups. The first dimensionless group of interest is a modified form of the Peclet number and is defined as

$$Pe_m = \frac{< v > H^2}{D_{ab} L} \,, \tag{4}$$

where $< v >$ is the average fluid velocity, H is the height of the channel, D_{ab} is the diffusivity of the solute and L is the length of the channel. This modified Peclet number, Pe_m, is a ratio of the characteristic diffusion time divided by the characteristic convection time. The second dimensionless group of interest is the height-to-length ratio, H/L. This group is small compared to unity, since the length is much larger than the height for the mixer designs under consideration. The range of Pe_m under investigation is 10 to 200. For a channel with a mixing length that is ten times the channel height, this Pe_m range corresponds to a Peclet number range of 100 to 2000. This Peclet number range is common in microfluidic devices. The final dimensionless group describes the distribution of zeta potential in the microfluidic channel. The zeta potential ratio is a ratio of the zeta potential in the mixing region of the channel divided by the average zeta potential in the channel and is defined as

$$\hat{\zeta} = \frac{\zeta_{mix} \sum_{j=1}^{N} L_j}{\sum_{j=1}^{N} \zeta_j L_j} \,, \tag{5}$$

where the subscripts denote the region in the channel.

Figure 1 illustrates an example mixer with four regions. Region 1 consists of the inlets. Inlet B has a given solute concentration and inlet A is solute free. Region two is the combined inlet stream. The length of the inlet stream is ten times the height of the channel. Region three is the mixing region and has a length that is ten times the height of the channel. The zeta potential in this region is varied to constrict the mixing steams. The fourth region is the outlet. The two black lines illustrate the locations where data are extracted to determine the EOM. The black lines are located a distance of one channel height before the mixing region and one channel height after the mixing region. For this analysis, the width and the height of the channel are constant. The figure illustrates the length of the mixing region. This length will be used in the Pe_m calculations. This figure also illustrates a sample result. In region 2, the two fluids meet and mix due to diffusion. In region 3, the mixing streams encounter a constriction that reduces the characteristic diffusion length and increases mixing. The constriction is due to recirculating velocity profiles within the mixing region. The zeta potential in the mixing region is opposite the zeta potential in the rest of the channel. When a electric potential is applied, the slip velocity along the walls of the mixing region is in the opposite direction of the overall average velocity for the channel.

Figure 2 illustrates the EOM versus zeta potential ratio for the electroosmotic flow mixer with varying modified Peclet number. As the zeta potential ratio decreases, the zeta potential in the mixing region decreases while the zeta potential in the rest of the channel remains fixed. If the zeta potential in the mixing region is opposite in sign of the zeta potential in the other regions,

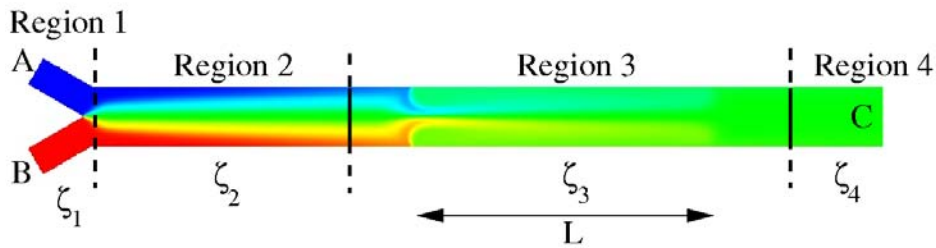

Figure 1: This figure illustrates the two-dimensional electroosmotic flow mixer. The channel geometry has three inlets/outlets. Inlet A is a stream without solute. Inlet B is a stream with solute. C is the outlet. The channel is made up of four separate regions. Each region is labeled along with the zeta potential for each region. Region 3 is the mixing region. The analysis points are illustrated on figure with two solid black lines. The lines are located one channel height before the mixing region and one channel height after the mixing region. Each line represents multiple nodes. Each node has a result for pressure, velocity, and concentration. The EOM is calculated using the concentration data from the nodes. This figure is not to scale.

recirculation will occur in the mixing region. The recirculations then constrict the mixing fluids leading to increased mixing. The EOM also increases with decreasing modified Peclet number. An increase in the modified Peclet number can be thought of as an increase in the average velocity of the mixing streams. By increasing the average velocity, the amount of time that the mixing streams spend in the mixing region decreases, resulting in a decrease in mixing. EOM is maximized by minimizing both the modified Peclet number and the zeta potential ratio. This work identifies that electroosmotic flow in channels with step changes in zeta potential can be effective mixers given the appropriate distribution of zeta potentials, determines key dimensionless groups for designing electroosmotic flow mixers and predicts EOM results.

3.1.2 Manipulating zeta potential using living-radical surface grafting

Based on previous work, electroosmosis with step changes in zeta potential can provide an effective mixer. However, fabricating step changes in zeta potential can be difficult. Since LRP has the necessary capabilities, a proof-of-concept study was performed to determine if the zeta potential of a surface can be manipulated using LRP to surface graft different materials. The experiment consisted of fabricating substrate samples and then surface grafting different materials on the substrate samples.

The substrate material was fabricated using a contact photopolymerization method (CLiPP) [4, 15]. The substrate consisted of 48.9 wt% triethylene glycol diacrylate (TEGDA, Sartomer), 48.9 wt% urethane diacrylate (Ebecryl 4827, UCB Chemicals), 0.98 wt% acrylic acid (AA, Aldrich), 0.49 wt% tetraethylthiuram disulfide (TED, Aldrich) and 0.73 wt% 2,2-dimethoxy-2-phenylacetophenone (DMPA, Ciba-Geigy). All materials were used as received. The materials were mixed using a sonicator and then the substrate was purged with Argon for 2 minutes. Small amounts of the substrate material (825 microL) were placed in contact with a polycarbonate support and a photomask. The substrate was polymerized for 500 seconds using the UV collimated light source at 45 mW/cm^2.

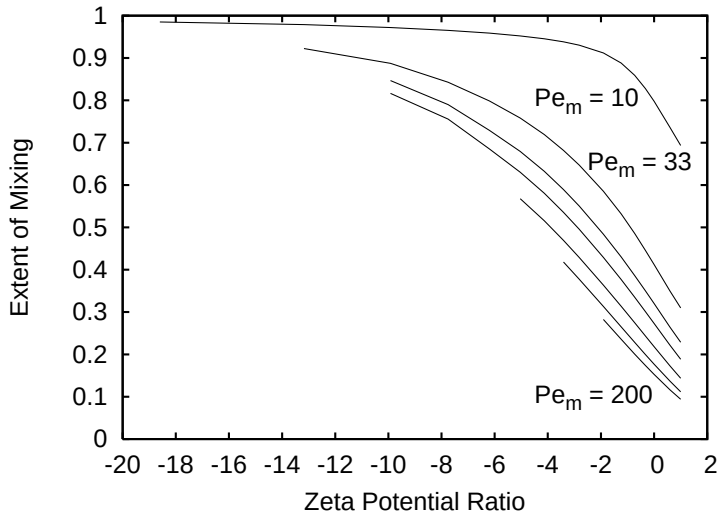

Figure 2: Extent of mixing (EOM) versus zeta potential ratio for a electroosmotic flow mixer. The length of the inlet stream (region 2) is ten times the height of the channel. The mixing region (region 3) has a length that is ten times the height of the channel. Each line represents a different modified Peclet number, Pe_m. In this figure, the modified Peclet number has values of 10, 33, 50, 66, 100, 150 and 200 (top to bottom). EOM increases with decreasing modified Peclet number and decreasing zeta potential ratio.

This exposure time ensured that the substrate material reached a conversion over 90%. Since the substrate contains dithiocarbamate (DTC) radicals from the TED, when the polymerization is stopped, the DTC radicals cap the propagating radicals in the material. Since the substrate material is fully mixed before polymerization, the surface concentration of the DTC radicals is assumed uniform. The samples were then washed with methanol to remove any unreacted species.

This project consisted of two studies. The first study investigated the use of two surface grafting materials. Both materials selected, poly(ethylene glycol) (PEG375, Aldrich) acrylate and 2-(Dimethylamino)ethyl methacrylate (DMAEMA, Aldrich), were purged with Argon for 2 minutes before use. A small quantity of each material (200 microL) was placed on the substrate samples and exposed to a 45 mW/cm^2 collimated illumination source for 900 seconds. Since neither of the materials contained initiator, the polymerization taking place was initiated by the DTC radicals on the surface of the substrate. After polymerization, each sample was washed with methanol and water to remove any unreacted material. The zeta potential of each sample was then tested over a pH range (5-8) using a ELS-8000 (Photal, Otsuka Electronics, Japan) that utilizes the electrophoresis method [42]. At least three samples were measured for each material. Each sample was measured twice. The second study focused on the zeta potential of DMAEMA surface grafted chains as a function of exposure time. A small quantity of DMAEMA (200 microL) was used to coat the polymerized substrate. The samples were then exposed to a 45 mW/cm^2 collimated light source for either 50, 100, 200, 450 or 900 seconds. After exposure, the samples were cleaned using methanol and water to remove any unreacted material. The samples were then tested using the ELS-8000 (Photal, Otsuka Electronics, Japan) over a range of pH (2-10). At least three samples were measured for each exposure time. Each sample was measured twice.

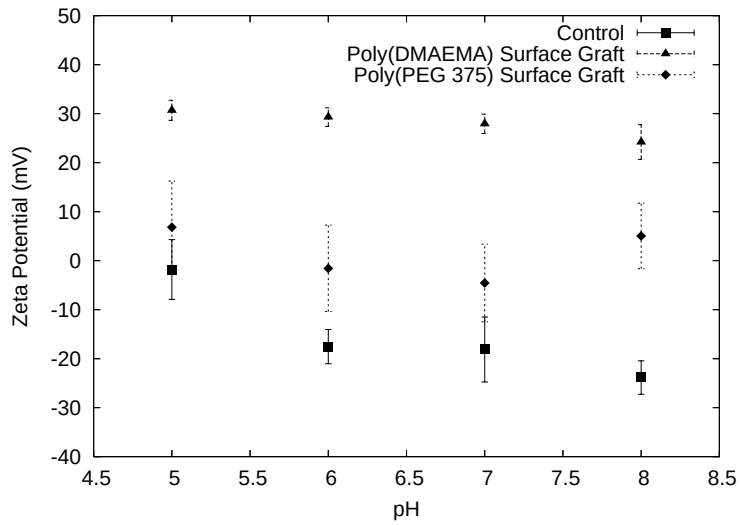

Figure 3: Zeta potential versus pH for the substrate (control), the substrate with a DMAEMA surface graft and the substrate with a PEG375 acrylate surface graft. The error bars represent the 90% confidence limits. The substrate was polymerized at 45 mW/cm^2 for 500 seconds. The surface grafts were polymerized at 45 mW/cm^2 for 900 seconds. The zeta potential measurements were conducted in a 10 mM KCl solution.

Figure 3 gives zeta potential versus pH for the substrate material, a PEG375 acrylate surface-grafted sample and a sample with a DMAEMA surface graft. The error bars represent the 90% confidence limits. The control material exhibits a negative zeta potential over the majority of the pH range. This zeta potential is the result of the AA in the material. Following polymerization of the substrate, a portion of the AA in the substrate resides on the surface. In the presence of a liquid, the AA on the surface donates protons, resulting in a negative surface charge. Over the entire pH range, the surface grafted PEG375 acrylate does not exhibit a zeta potential statistically different from 0 mV. The PEG375 acrylate completely covers the surface of the substrate, effectively isolating the AA in the substrate from the electrolyte solution. Since PEG375 acrylate does not contain functional groups that donate or accept protons, this result of a neutral surface is expected. The final material considered in controlling surface charge was DMAEMA. The results illustrate that the surface grafted DMAEMA exhibits a positive zeta potential over the entire pH range. The amino groups in the DMAEMA molecules can accept protons in the presence of an electrolyte, resulting in a positive zeta potential.

Figure 4 gives zeta potential versus pH for a control surface and a control surface with a DMAEMA surface graft. Each data set represents a different exposure time, ranging from 0 to 900 seconds, with the error bars illustrating the 90% confidence limits. At low exposure times, the zeta potentials of the control substrate and the substrate with the DMAEMA surface graft are not statistically different, indicating that the surface coverage of DMAEMA molecules is not large enough to measure. After 200 seconds, the zeta potential of the surface graft is statistically different from that of the control, suggesting that the coverage of the DMAEMA molecules is significant. Finally, after 450 and 900 second exposure times, the grafted sample zeta potentials are statistically different from the 200 seconds, but are not statistically different from each other. These results sug-

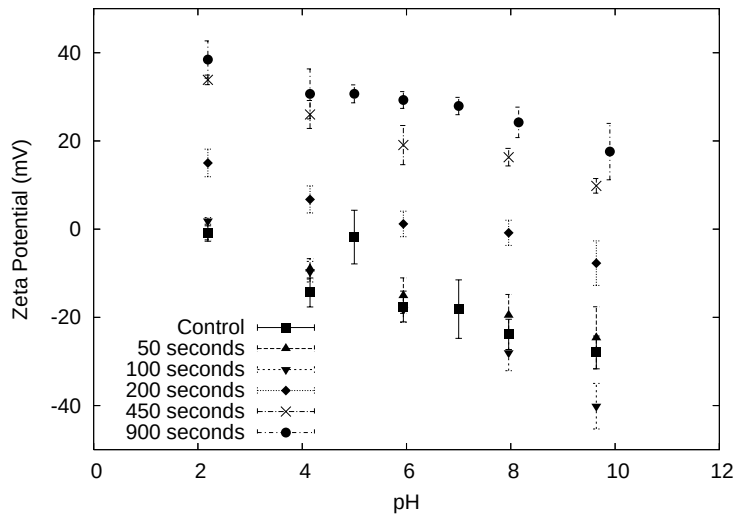

Figure 4: Zeta potential versus pH for substrate surface grafted with DMAEMA for various exposure times. The error bars represent the 90% confidence limits. The substrate was polymerized at 45 mW/cm^2 for 500 seconds. The surface grafts were polymerized at 45 mW/cm^2 for 0 (Control), 50, 100, 200, 450 and 900 seconds. The zeta potential measurements were conducted in a 10 mM KCl solution.

gests that for exposure times greater than 100 seconds and below 450 seconds, the zeta potential of the surface is a combination of the AA in the substrate and the surface-grafted DMAEMA. Above exposure times of 450 seconds, the surface of the material is completely covered with DMAEMA. Based on these results, LRP surface grafting is an effective method for manipulating zeta potential.

3.2 Mixing using hydrodynamic focusing

The hydrodynamic focusing mixer geometry is illustrated in figure 5. The hydrodynamic focusing mixer operates on the same principle as the previously described electroosmotic flow mixer. However, instead of constricting the mixing streams using recirculating flow profiles, the hydrodynamic focusing mixer uses a side stream to constrict the mixing streams. The mixer has five regions, three inlets and two outlets. Inlet B contains a solute. Inlet A is solute free. The side channel has an inlet C and an outlet D. The flow-rate for inlet C equals the flow-rate for outlet D for all of the simulation conditions. The flow-rate of outlet E is therefore equal to the flow-rates of A plus B. The flow-rates of A and B are equal. The length of the mixing region is ten times the height of the channel and is illustrated with the double arrow labeled L. The two black lines illustrate the analysis points for the EOM calculations. The black lines are located a distance of one channel height before the mixing region and one channel height after the mixing region. Region 5 is a loop side channel that connects the outlet of the side channel, D, to the inlet of the side channel, C. The heights and widths of the main channel and the side channel are equal. The two dimensionless groups of interest are the modified Peclet number (defined in section 3.1.1) and the ratio of the volumetric flow-rate of the side channel divided by the volumetric flow-rate of the main channel.

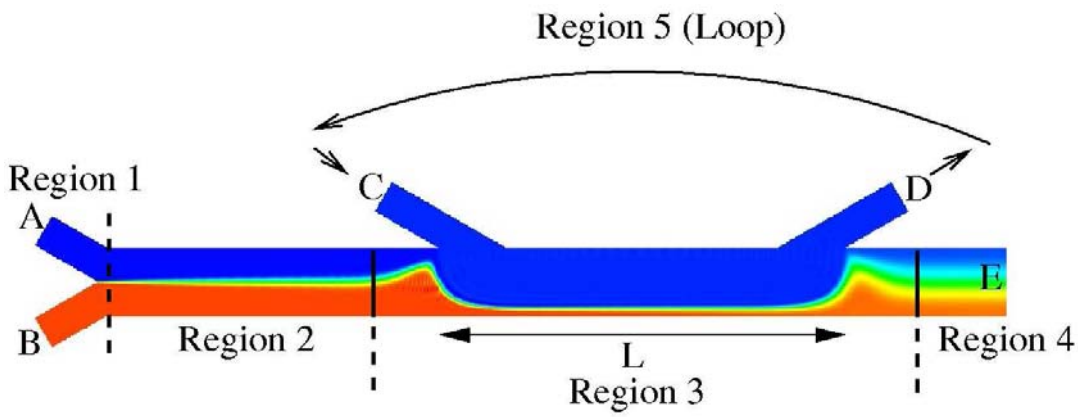

Figure 5: This figure illustrates the two-dimensional hydrodynamic focusing mixer. The channel geometry has five inlets/outlets. Inlet A is stream without solute. Inlet B is a stream with solute. Inlet C is an inlet. D and E are outlets. The channel has five labeled regions. Region 5 is the loop side channel and is not shown. The analysis points are illustrated on figure with two solid black lines. The analysis lines are located one channel height before the mixing region and one height after the mixing region. Each line represents multiple nodes. Each node has a result for pressure, velocity, and concentration. The concentration of the side channel outlet is averaged and then used as the side channel inlet boundary condition for the next iterations. The iterations continue until the difference in the average side channel outlet concentration for subsequent iterations is less than 0.01%. This figure is not to scale.

The EOM for the hydrodynamic focusing mixer is calculated the same way as the electroosmotic flow mixer (see section 3.1.1).

This study used GOMA to solve the two-dimensional equations for continuity, Navier-Stokes and mass transfer with the appropriate boundary conditions. At the walls of the channel, the normal component of velocity is zero, the tangential component is zero, and solute flux is zero. At the inlet of the main channel and the side channel, the inlet velocity profile is parabolic.

Diffusion of the solute into the side channel occurs at certain flow-rate ratios and modified Peclet numbers. The concentration of the side channel outlet is averaged and then used as the side channel inlet boundary condition for the next iterations. The iterations continue until the difference in the average side channel outlet concentration for subsequent iterations is less than 0.01%.

Figure 6 illustrates EOM versus the flow-rate ratio between the side channel and the main channel for various modified Peclet numbers. For a constant modified Peclet number, the EOM increases with increasing flow-rate ratio. As the flow-rate ratio increases, the constriction the two mixing fluids encounter decreases. By constricting the fluids, the characteristic diffusion length decreases and mixing increases. As the modified Peclet number increases, the EOM decreases. Increasing the modified Peclet number can be thought of as increasing the average velocity of the mixing streams. By increasing the modified Peclet number, the amount of time the mixing fluids spend in the mixing region decreases, resulting in lower mixing. The EOM is maximize by high flow-rate ratios and low modified Peclet numbers.

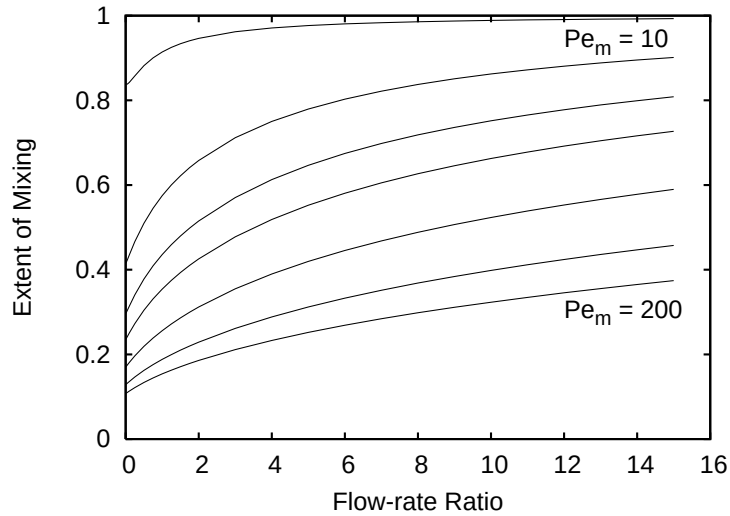

Figure 6: Extent of mixing (EOM) versus flow-rate ratio for a hydrodynamic focusing mixer with a loop side channel. The length of the inlet stream (region 2) is ten times the height of the channel. The mixing region (region 3) has a length that is ten times the height of the channel. Each line represents a different modified Peclet number, Pe_m. In this figure, the modified Peclet number has values of 10, 33, 50, 66, 100, 150 and 200 (top to bottom). EOM increases with decreasing modified Peclet number and increasing flow-rate ratio.

3.3 Mixing using physical constrictions

This mixer design uses a physical constriction and is illustrated in figure 7. The mixer has four regions. Region 1 consists of the inlets. Inlet B has a given solute concentration and inlet A is solute free. Region two is the combined inlet stream. The length of the inlet stream is ten times the height of the channel. Region three is the mixing region and has a length that is ten times the height of the unconstricted channel. The height is this region will be varied to constrict the mixing steams. The fourth region is the outlet. The two black lines illustrate the locations where data are extracted to determine the EOM. The black lines are located a distance of one unconstricted channel height before the mixing region and one unconstricted channel height after the mixing region. The two dimensionless groups of interest are the modified Peclet number (defined in section 3.1.1) and the ratio of the height of the mixing region divided by the height of the rest of the channel. The EOM for the hydrodynamic focusing mixer is calculated the same way as for the electroosmotic flow mixer (see section 3.1.1).

This problem was solved using GOMA and the two-dimensional equations for continuity, Navier-Stokes and mass transfer. At the walls of the channel, the normal component of velocity is zero, the tangential component of velocity is zero, and no solute flux occurs. At the inlets of the channel, the velocity profile is parabolic.

Figure 8 illustrates the EOM versus height ratio for various modified Peclet numbers. As the height ratio decreases, the height of the mixing region decreases, resulting in higher EOM. As the modified Peclet number decreases, the amount of time the mixing fluids spend constricted

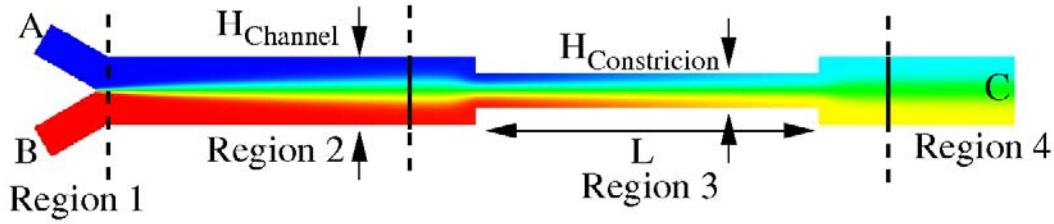

Figure 7: This figure illustrates the physical constriction mixer. The channel geometry has three inlets/outlets. Inlet A is stream without solute. Inlet B is a stream with solute. C is the outlet. The channel is made up of four regions. Region 3 is the mixing region. The height of the channel and the height of the constriction are labeled. The analysis points are illustrated on figure with two solid black lines. The analysis lines are located one unconstricted channel height before the mixing region and one unconstricted channel height after the mixing region. Each line represents multiple nodes. Each node has a result for pressure, velocity, and concentration. The EOM is calculated using the concentration data from the nodes. This figure is not to scale.

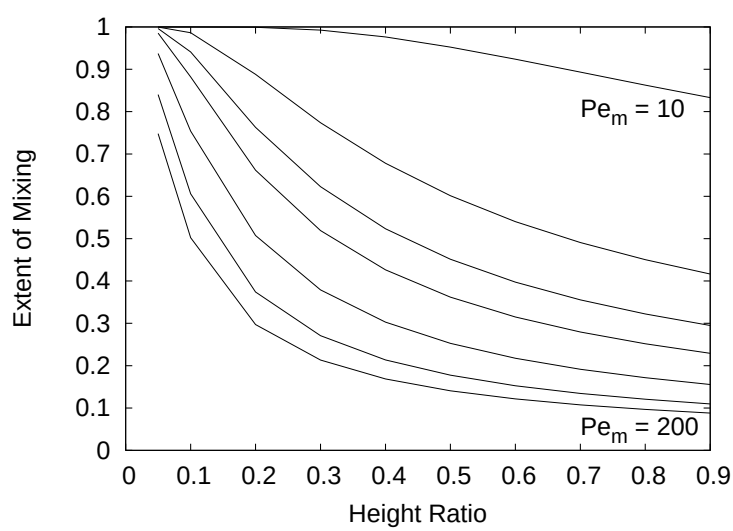

Figure 8: Extent of mixing (EOM) versus height ratio for a physical constriction mixer. The length of the inlet stream (region 2) is ten times the height of the channel. The mixing region (region 3) has a length that is ten times the height of the channel. Each line represents a different modified Peclet number, Pe_m. In this figure, the modified Peclet number has values of 10, 33, 50, 66, 100, 150 and 200 (top to bottom). EOM increases with decreasing modified Peclet number and decreasing height ratio.

increases, resulting in increased mixing. The EOM is maximized at low height ratios and low modified Peclet numbers.

3.4 Mixing using porous polymer monoliths

3.4.1 Monolith Fabrication

Porous polymer monoliths were fabricated using a technique described in Simms et. al. [41]. The fabrication technique uses a mixture of salt crystals and photopolymerizable monomer to fabricate the monoliths. The monomer is the same material that is used to fabricate microfluidic devices. See section 3.1.2 for a description of the substrate composition. The salt crystals are sieved to isolate a given crystal size range. For these experiments, two salt crystal size ranges were chosen; 75 to 106 microns and 53 to 180 microns. The concentration of the salt in the monomer is 80 wt%. After mixing the salt and monomer, the resulting paste is packed into microfluidic trenches that are 400 microns x 400 microns. The trench configuration consists of two inlets that converge into a single outlet in a "Y" configuration. The paste is packed into the trench at the convergence point. The paste is polymerized for 500 seconds using a 45 mW/cm^2 collimated light source. The photomask used to polymerize the paste controls the length of the monolith. For these experiments, the monolith length is 2 mm. After polymerization, the microfluidic trench that includes the monolith is submerged in DI water for two days. During this time, the salt crystals dissolve, resulting in an interconnected pore network. Once the salt is dissolved, the monolith is allowed to dry and a lid is fabricated on the device using the standard CLiPP process. The resulting devices require cleaning to remove any monomer. Compressed air is forced through the channels to remove any monomer. Next, needles are glued into the channels to allow for connection to syringe pumps. To remove the rest of the monomer, DI water is pumped through the channels. Typically, it is necessary pump water through the channels for 3 days. The mixers are considered clean when monomer no longer flows out of the porous polymer monolith.

3.4.2 Extent of Mixing Experiments

The EOM for the porous polymer monolith mixers was measured by determining the change in the concentration profile of a fluorescent dye due to the mixer. One inlet stream consists of a 0.3 microM solution of Fluorescein (Sigma) in phosphate buffered saline (pH 8). The second inlet stream consists of only phosphate buffered saline (pH 8). Phosphate buffered saline is used to minimize any pH drift over the course of the experiment. The extent of mixing is determined by measuring the distribution of the fluorescent dye at the inlet and outlet of the porous polymer monolith using a photomultiplier tube system (PTI 814) and an inverted microscope (Nikon TE300). The photomultiplier tube system is setup to scan across the channel before and after the plug. The resulting data are intensity versus position sets. The concentration and the intensity of the Fluorescein dye are linearly related at the concentration, pH, and photomultiplier aperture setting used. Extent of mixing is determined by examining the difference in intensity at the 1/3 and 2/3 channel width positions. Mathematically, the difference is

$$\Delta = C_{\frac{1}{3}} - C_{\frac{2}{3}} \ . \tag{6}$$

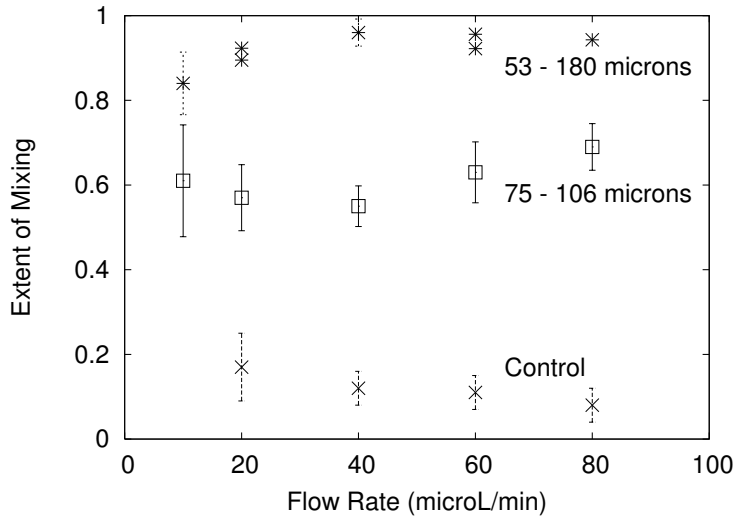

Figure 9: Extent of mixing versus flow-rate for porous polymer monolith mixers. The control data set is for a straight channel without a polymer monolith. Two different monolith data sets are provided, each with a different pore size distribution. For the conditions investigated, the extent of mixing increases with increasing monolith heterogeneity, but is independent of the flow-rate.

A difference can be calculated before the plug, ΔI, and after the plug, ΔO. The extent of mixing is then calculated as

$$\mathrm{EOM} = 1 - \frac{\Delta O}{\Delta I} \,. \tag{7}$$

The flow-rates investigated are 10 microL/min to 80 microL/min.

Figure 9 illustrates the EOM versus flow-rate data for porous polymer monoliths and for a channel without a monolith (control). The conditions with at least three repeats include error bars that define the 90% confidence limits. Two different salt crystal size ranges are illustrated. These two salt crystal size ranges were chosen in order to fabricate porous polymer monoliths with different heterogeneity. With a larger range of pore sizes, the monoliths fabricated using the 53 - 180 micron salt crystal size range is more heterogeneous. For the conditions investigated, the EOM is highest for the most heterogeneous monolith. Heterogeneous monoliths break up the two laminar fluid streams and cause them to intermingle. By increasing the heterogeneity, the monolith contain a wider range of random local velocities that are more effective at intermingling the two mixing streams. These results agree with previous research where the authors used phase separation to fabricate porous monolith and found that mixing was maximized when the pores within the monoliths were large and irregular [36]. Also, for these conditions, the EOM does not depend on the flow-rate of the fluid. As the flow- rate increases, the residence time for the mixing fluids in the porous monolith decreases. To counteract the decrease in residence time, the effective dispersivity must have increased to maintain a constant EOM. This result agrees with previous research performed by Koch and Brady [43], where the authors determined that, for moderate Peclet numbers, the effective dispersivity of a fixed bed or porous media to be proportional to the average fluid velocity. The authors conclude that, at the Peclet numbers in question, convection plays a more significant role than diffusion of the solute and that the dispersion is the result of a

stochastic velocity field within the porous polymer plug. Typically for microfluidic devices, the flow is laminar in nature; however, in porous media, the enhanced dispersion is the result of the random nature of the pores within the plug.

4 Recommendations

4.1 Porous polymer monoliths

To better understand porous polymer monolith mixers, additional experiments should be performed. Future experiments should focus on additional monolith lengths. Previously experiments were performed to investigate a 2 mm (discussed in section 3.4) porous monolith and a 4 mm porous monolith fabricated using 75 - 106 micron salt crystals. The experiments with the 4 mm monolith were unsuccessful. The pressure drop required to pump fluid through the longer plug was very high. The high pressure caused either device or pump failure. Future experiments should investigate shorter monoliths to better understand the role of monolith length in microfluidic mixing.

4.2 Hydrodynamic focusing mixer

Based on the simulation work presented in section 3.2, experiments should be performed to evaluate hydrodynamic focusing mixers. The same experimental procedure as the one used in section 3.4.2 could be used to evaluate the mixer. Various volumetric flow-rate ratios and modified Peclet numbers should be investigated. The overall goal of this recommended work is to determine the characteristic design rules for mixers using hydrodynamic focusing and verify simulation results.

4.3 Microfluidic mixer comparison

Sections 3.1.1, 3.2 and 3.3 discussed progress on simulating three microfluidic mixing techniques. The recommendations for this project is to expand the simulations and consider the energy requirements for each mixer. The energy requirement will depend on the channel configuration as well as the desired EOM. A rigorous dimensional analysis should be performed on the three mixer designs to appropriately compare them to one another. Once the energy requirements are understood, the mixers could then be compared and design rules developed to facilitate the selection of mixer techniques for a given application. In addition, simulations should be preformed on a long straight channel without a mixer. This channel would be the reference point that the other mixers should be compared to. The overall goal of this project would be to provide information that will help microfluidic device designers select the appropriate mixer technique (if any) and predict the expected EOM and energy requirements of the chosen mixer.

References

[1] N.-T. Nguyen, S. T. Wereley, Fundamentals and applications of microfluidics, Artech House, 2002.

[2] G. M. Whitesides, A. D. Strock, Flexible methods for microfluidics, Physics Today 54 (2001) 42–48.

[3] D. J. Beebe, G. A. Mensing, G. M. Walker, Physics and applications of microfluidics in biology, Annual Review of Biomedical Engineering 4 (2002) 261–286.

[4] K. T. Haraldsson, J. B. Hutchison, R. P. Sebra, B. T. Good, K. S. Anseth, C. N. Bowman, 3d polymeric microfluidic device fabrication via contact liquid photolithographic polymerization (clipp), Sensors and Actuators Part B: Chemical 113 (2006) 454–460.

[5] J. C. McDonald, D. C. Duffy, J. R. Anderson, D. T. Chiu, H. K. Wu, O. J. A. Schueller, G. M. Whitesides, Fabrication of microfluidic systms in poly(dimethylsiloxane), Electrophoresis 21 (2000) 27–40.

[6] H. Becker, C. Gartner, Polymer microfabrication methods for microfluidic analytical applications, Electrophoresis 21 (2000) 12–26.

[7] H. Becker, L. E. Locascio, Polymer microfluidic devices, Talanta 56 (2002) 267–287.

[8] M. E. Staben, A. Z. Zinchenko, R. H. Davis, Motion of a particle between two parallel plane walls in low-reynolds-number poiseuille flow, Physics of Fluids 15 (2003) 1711–1733.

[9] N. T. Nguyen, X. Y. Huang, T. K. Chuan, Mems-micropumps: a review, Journal of Fluids Engineering - Transactions of the ASME 124 (2002) 384–392.

[10] L. Kricka, P. Wilding, Micromachining: a new direction for clinical analyzers, Pure Appl. Chem. 68 (1996) 1831–1836.

[11] A. Manz, C. S. Effenhauser, N. Burggraf, D. J. Harrison, K. Seiler, K. Fluri, Electroosmotic pumping and electrophoretic separations for miniaturized chemical analysis systems, J. Micromech. Microeng. 4 (1991) 257–265.

[12] R. F. Ismagilov, A. D. Stroock, P. J. A. Kenis, G. Whitesides, H. A. Stone, Experimental and theoretical scaling lasw for transverse diffusive broadening in two-phase laminar flows in microchannels, Appl. Phys. Lett. 76 (2000) 2376.

[13] N.-T. Nguyen, Z. Wu, Micromixers - a review, J. Micromech. Microeng. 15 (2005) R1–R16.

[14] V. Hessel, H. Löwe, F. Schönfeld, Micromixers - a review on passive and active mixing principles, Chemical Engineering Science 60 (2005) 2479 – 2501.

[15] J. B. Hutchison, K. T. Haraldsson, B. T. Good, R. P. Sebra, N. Luo, K. S. Anseth, C. N. Bowman, Robust polymer microfluidic device fabrication via contact liquid photolithographic polymerization (clipp), LAB ON A CHIP 6 (2004) 658–662.

[16] D. Long, H. A. Stone, A. Ajdari, Electroosmotic flows created by surface defects in capillary electrophoresis, J. Colloid Interface Sci. 212 (1999) 338–349.

[17] M. H. Oddy, J. G. Santiago, J. C. Mikkelsen, Electrokinetic instability micromixing, Anal. Chem. 73 (2001) 5822–5832.

[18] N. Luo, A. T. Metters, J. B. Hutchison, C. N. Bowman, K. S. Anseth, A methacrylated photoiniferter as a chemical basis for microlithography: micropatterning based on photografting polymerization, Macromolecules 36 (2003) 6739–6745.

[19] N. Luo, J. B. Hutchison, K. S. Anseth, C. N. Bowman, Surface-initiated photopolymerization of poly(ethylene glycol) methyl ether methacrylate on a diethyldithiocarbamate-mediated polymer substrate, Macromolecules 35 (2002) 2487–2493.

[20] N. Luo, J. B. Hutchison, K. S. Anseth, C. N. Bowman, Synthesis of a novel methacrylic monomer iniferter and its application in surface photografting on crosslinked polymer substrates, J Polym Sci Part A: Polym Chem 40 (2002) 1885–1891.
[21] B. Jo, L. V. Lectureship, K. Motherhood, D. Beebe, Three-dimensional micro-channel fabrication in polydimethylsiloxane(pads), J. Microelectromech. 9 (2000) 76–81.
[22] H. Ma, L. F. Hakim, C. N. Bowman, R. H. Davis, Factors affecting membrane fouling reduction by surface modification and backpulsing, J. Membr. Sci. 189 (2001) 255–270.
[23] S. K. Reddy, R. P. Sebra, K. S. Anseth, C. N. Bowman, Living radical photopolymerization induced grafting on thiol-ene based substrates, J. Polym Sci Part A: Polym Chem 43 (2004) 2134–2144.
[24] Y. Nakayama, J. M. Anderson, T. Matsuda, Laboratory-scale mass production of a multi-micropatterned grafted surface with different polymer regions, J Biomed Mater Res 53 (2000) 584–591.
[25] H. J. Lee, Y. Nakayama, T. Matsuda, Spatio-resolved, macromolecular architectural surface: highly branched graft polymer via photochemically driven quasiliving polymerization technique, Macromolecules 32 (1999) 6989–6995.
[26] B. de Boer, H. K. Simon, M. P. L. Werts, E. W. van der Vegte, G. Hadziioannou, ”living” free radical photopolymerization initiated from surface-grafted iniferter monolayers, Macromolecules 33 (2000) 349–356.
[27] C. M. Brotherton, R. H. Davis, Electroosmotic flow in channels with step changes in zeta potential and cross section, J. Colloid Interface Sci. 270 (2004) 242–246.
[28] E. Biddiss, D. Erickson, D. Li, Heterogeneous surface charge enchanced micromixing for electrokinetic flows, Anal Chem 76 (2004) 3208–3214.
[29] D. Erickson, D. Li, Influence of surface heterogeneity on electrokinetically driven microfluidic mixing, Langmuir 18 (2002) 1883–1892.
[30] C.-C. Chang, R.-J. Yang, Computational analysis of electrokinetically driven flow mixing in microchannels with patterned blocks, J. Micromech. Microeng. 14 (2004) 550–558.
[31] H.-Y. Wu, C.-H. Liu, A novel electrokinetic micromixer, Sensors and Actuators A 118 (2005) 107–115.
[32] F. Tian, B. Li, D. Y. Kwok, Tradeoff between mixing and transport in electroosmotic flow in heterogeneous microchannels with nonuniform surface potentials, Langmuir 21 (2005) 1126–1131.
[33] K. Jensen, Chemical kinetics: smaller, faster chemistry, Nature 393 (1998) 735–736.
[34] J. B. Knight, A. Vishwanath, J. P. Brody, R. H. Austin, Hydrodynamic focusing on a silicon chip: mixing nanoliters in microseconds, Phys. Rev. Lett. 80 (1998) 3863–3866.
[35] T. T. Veenstra, T. S. J. Lammerink, M. C. Elwenspoek, A. van den Berg, Characterization method for a new diffusion mixer applicable in micro flow injection analysis systems, J. Micromech. Microeng. 9 (1999) 199–202.
[36] T. Rohr, C. Yu, M. H. Davey, F. Svec, J. M. J. Fréchet, Porous polymer monoliths: simple and efficient mixers prepared by direct polymerization in the channels of microfluidic chips, Electrophoresis 22 (2001) 3959–3967.
[37] T. Rohr, E. F. Hilder, J. J. Donovan, F. Svec, J. M. J. Fréchet, Photografting and the control of surface chemistry in three-dimensional porous polymer monoliths, Macromolecules 36 (2003) 1677–1684.
[38] J. Moorthy, D. J. Beebe, In situ fabricated porous filters for microsystems, Lab on a Chip 3

(2003) 62–66.
[39] C. Yu, F. Svec, J. M. J. Fréchet, Towards stationary phases for chromatography on a microchip: molded porous polymer monoliths prepared in capillaries by photoinitiated in situ polymerization as separation media for electrochromatography, Electrophoresis 21 (2000) 120–127.
[40] C. Yu, M. Xu, F. Svec, J. M. J. Fréchet, Preparation of monolithic polymers with controlled porous properties for microfluidic chip applications using photoinitiated free-radical polymerization, J. Polym Sci Part A: Polym Chem 40 (2002) 755–769.
[41] H. M. Simms, C. M. Brotherton, B. T. Good, K. S. Anseth, C. N. Bowman, In situ fabrication of macroporous polymer networks within microfluidic devices by living radical photopolymerization and leaching, Lab on a Chip 5 (2005) 151–157.
[42] Y. Shim, H.-J. Lee, S. Lee, S.-H. Moon, J. Cho, Effects of natural organic matter and ionic species on membrane surface change, Environ. Sci. Technol. 36 (2002) 3864–3871.
[43] D. L. Koch, J. F. Brady, Dispersion in fixed beds, J. Fluid Mech. 154 (1985) 399–427.

DISTRIBUTION:

2 MS 9018
Central Technical File, 8944

2 MS 0899
Technical Library, 4536

1 MS 0188
Chavez, D., LDRD Office, 1030

1 MS 0824
Hermina, W., 1510

1 MS 0834
Lash, J., 1514

1 MS 0834
Schunk, P.R., 1514

1 MS 0834
Hopkins, M.M., 1514

1 MS 0834
Grillet, A.M., 1512

1 MS 0834
Bourdon, C., 1512

1 MS 0834
Brooks, C., 1512

1 MS 1080
Galambos, P., 1769

1 MS 1080
James, C.D., 1769

1 MS 1425
Branch, D.W., 1714

1 MS 0735
Ho, C., 6115

1 MS 9409
Rush, B.M., 8757

1 Robert Davis
Christopher Brotherton
Department of Chemical and Biological Engineering
University of Colorado
424 UCB, ECCH 111
Boulder, CO 80309-0424